ROVER-BASED RECONNAISSANCE WITH THERMAL INFRARED HYPERSPECTRAL IMAGING. A. D. Rogers[1], C. I. Honniball[2], T. D. Glotch[1], R. J. Hopkins[1], P. G. Lucey[3], D. Piquero[4], B. Wolfe[4], and K. E. Young[2]. [1]Stony Brook University (Stony Brook, NY, USA, deanne.rogers@stonybrook.edu), [2]NASA Goddard Space Flight Center, Greenbelt, MD [3]University of Hawaii, Honolulu, HI. [4]Spectrum Photonics, Inc., Honolulu, HI.

Introduction: The Artemis III candidate science program envisioned by [1] nominally includes the acquisition of *in-situ* compositional information to support sample selection activities. Spectral imaging provides a means for rapid compositional assessment, site documentation, and sample selection, and provides a critical link in scale between orbital spectral imaging and samples, as described in detail in [2-7]. A rover-mounted hyperspectral imager could acquire data that are processed and delivered for analysis by a "backroom" support team or the EVA crew. Here we build on previous efforts [2-5] by presenting example data products derived from hyperspectral thermal infrared (TIR) imaging at lunar-relevant analog terrains and demonstrate their potential use in meeting Artemis III science objectives.

Field location and imaging sites: Data were collected from Kilbourne Hole, New Mexico, during November 2021 as part of the field activities of the Remote, In Situ and Synchrotron Studies for Science and Exploration-2 (RISE2) sub-node of the NASA Solar System Exploration Research Virtual Institute (SSERVI). Kilbourne Hole is a maar crater that contains rhyolitic ash fall deposits, base surge deposits, paleosols, basaltic lava flows and abundant mantle/crustal xenoliths [e.g. 2 & refs. therein].

Vibrational spectroscopy: Molecular vibrations in minerals, glasses and volatiles give rise to distinctive spectral features in the ~2-100 μm range [e.g., 12]. Within the TIR region covered in this study (~7-14 μm), vibrational spectra are highly sensitive to changes in bulk silica content [11] and to various silicate, sulfate, carbonate, aluminum oxide and (a limited number of) iron oxide minerals [e.g., 12].

Instrument and Data Processing: A tripod-mounted hyperspectral imager from Spectrum Photonics, Inc. was used to measure thermal radiance between ~7-14 μm (ex., **Fig. 1)**. Spectral sampling is selectable; for most images spectral sampling was set to ~15 cm^{-1} resulting in 41 spectral channels. Images shown in this work were acquired at a focus distance of ~3 or ~10 m resulting in pixel sizes of ~3 or 10 mm at focus distance. The horizontal field of view is selectable and ranges up to 180°.

Calibrated radiance was obtained by measuring blackbody targets at two temperatures before each scene acquisition, following the methods of [8 & refs. therein]. Temperature-emissivity separation was calculated using the emissivity normalization method [9], with maximum emissivity set to 0.98. Mineral concentration maps were produced using non-negative linear spectral unmixing [10] and a spectral library of candidate igneous minerals and alteration products.

Example data products: A variety of reduced data products could be used depending on the specific needs and science objectives at the EVA site. False color images derived from principal components analysis (PCA **Fig. 2b**, and related method, decorrelation stretch (DCS) [13] (**Fig. 1**)) provide a survey of bulk compositional variations that could be used to quickly establish a subset of samples that capture the range of compositions present at the site. Science objectives that require sampling of specific lithologies (e.g. to test planetary differentiation hypotheses, to trace samples to specific impact basins, etc) could utilize mineral abundance or spectral index maps that locate specific materials of interest (e.g. **Fig. 2c-d**). Spectral matching algorithms [e.g. 14] can be used to rapidly identify spectrally unique materials that have not been encountered in previous sites (**Fig. 3**). Last, full spectral data cubes provide information-rich data sets that could be used in post-EVA detailed site

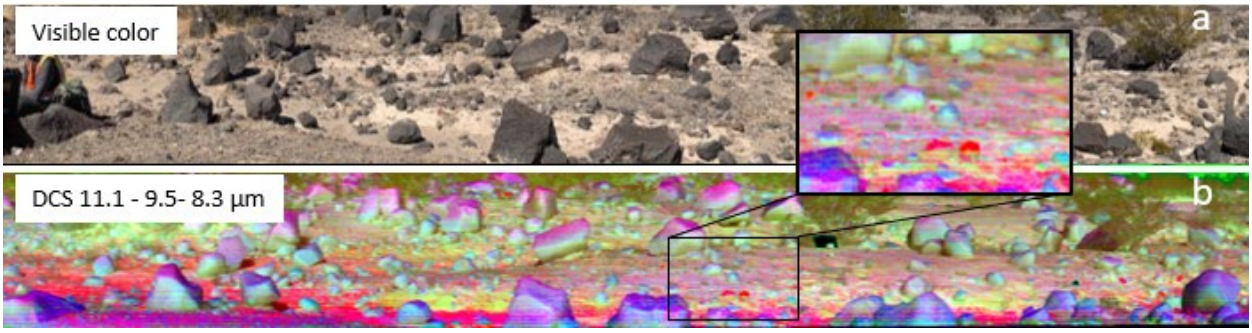

Fig. 1. **(a)** Visible panorama of boulders, small clasts, soils, desert pavement, and sparse vegetation. **(b)** Decorrelation stretched (DCS) image using radiance at 11.1, 9.5, and 8.3 μm displayed as red, green and blue. Color variations indicate compositionally distinct materials. Area in inset is ~10 m distance from sensor. Abundant olivine and pyroxenite xenoliths (cyan) and silicic clasts (red) are found among larger basaltic boulders (purple and pink).

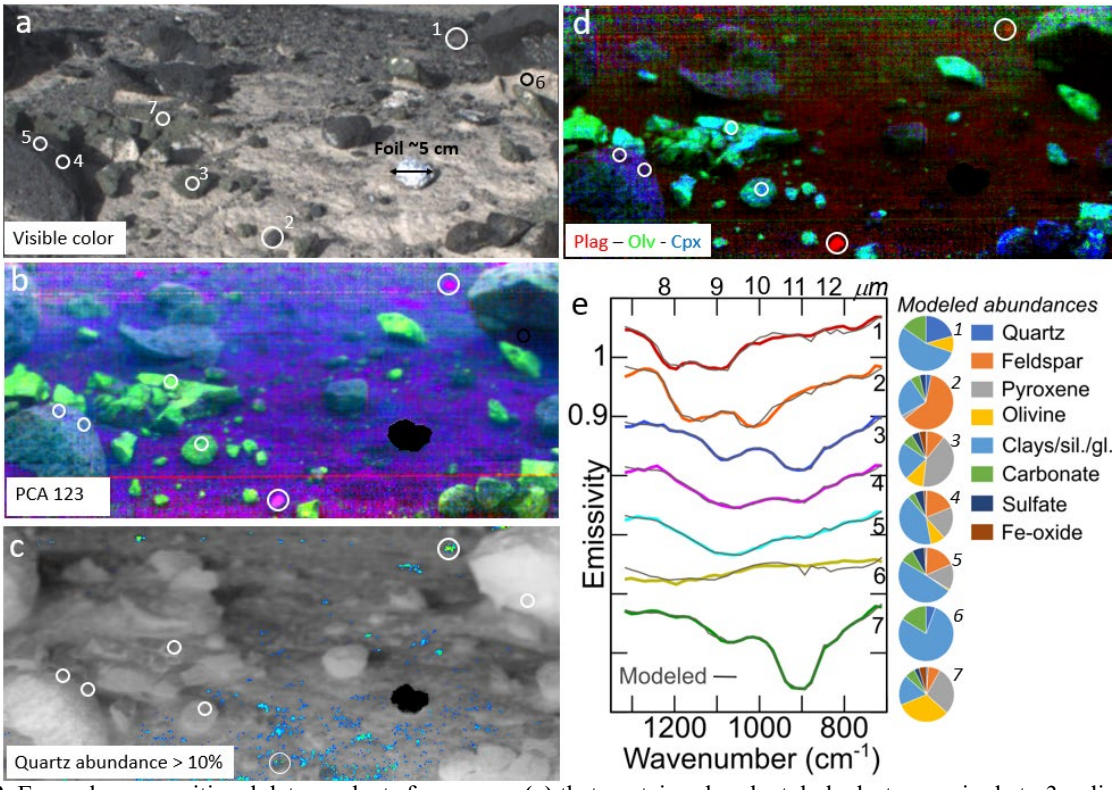

Fig. 2. Example compositional data products from scene **(a)** that contains abundant dark clasts, acquired at ~3m distance. Many clasts are visually similar, but spectrally distinctive in the infrared indicating compositional differences. Circles show locations of spectral extractions shown in (e). **(b)** Emissivity PCA bands 1-2-3; color variations indicate differences in bulk composition. (**c**) Quartz abundance greater than 10% (color) overlain on temperature image. **(d)** Mineral abundance maps displayed as an RGB composite, with plagioclase shown in red, olivine in green and clinopyroxene in blue. **(e)** Emissivity spectra extracted from areas highlighted by the different data products shown in b-d.

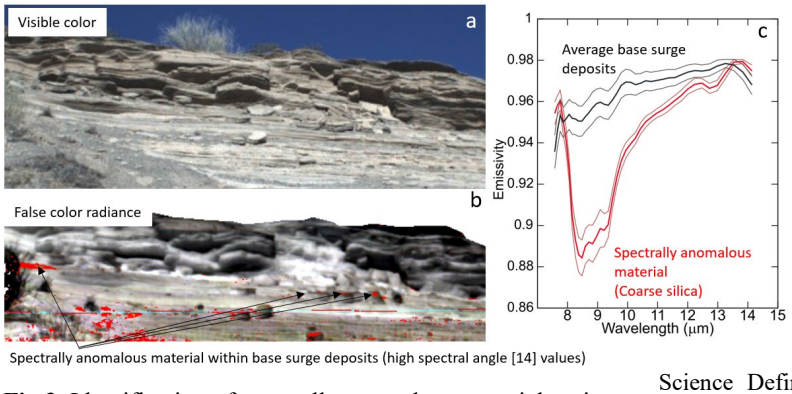

Fig.3. Identification of spectrally anomalous materials using a spectral matching algorithm to locate areas that do *not* match the avg. base surge deposits spectrum. **(a)** Visible image of base surge deposits. **(b)** Thermal radiance image. Red pixels are areas that do not spectrally match average base surge deposits. **(c)** Emissivity spectra of average base surge deposits and anomalous material (coarse silica).

documentation and geological analyses. For example, spectral images of impact breccia blocks or crater walls could be used to help characterize the lithologies present (e.g. **Fig. 2e**) and their geologic/petrologic context.

Conclusion: Diverse lithologies are not consistently visually recognizable. Hyperspectral infrared imaging can be used at a range of scales to aid in sampling, site documentation, and traverse planning and reduces risk of overlooking unique or key samples.

Acknowledgments: This work was funded by NASA SSERVI through a cooperative agreement to Stony Brook Univ.

References: [1] NASA (2020) Artemis III Science Definition Team report, NASA/SP-20205009602. [2] Ito, G. et al. (2018), *ESS, 5:21*, 10.1029/ 2018ea000375 [3] Young, K. et al., (2018) *ESS, 5:24,* 10.1029/ 2018ea000378. [4] Honniball, C. I. et al. (2020), *Lunar Surf. Sci. Wkshp*, Abs. 5079. [5] Honniball C. et al. (2020) Artemis III SDT White Paper #2041 [6] Tkaczyk, T. (2020), Artemis III SDT White Paper #2028 [7] Hewagama, T. (2020), Artemis III SDT White Paper #2110 [8] Ruff et al. (1997), *JGR 102*, 14899-14913 [9] Realmuto (1990), *Proc. 2nd TIMS Wkshp, JPL Pub. 90-55*, 26–30 [10] Lawson. & Hanson 1974 *Solving Least-Squares Problems.* Prentice-Hall [11] Hook et al. (2005) *RSE, 95,* 273-289 [12] Christensen et al. (2000), *JGR,105,* 9735-9739 [13] Gillespie et al. (1986) *RSE, 20*, 209-235 [14] Kruse et al. (1993) *RSE 44,* 145-163.